Quaternary Science Reviews 266 (2021) 107068

Contents lists available at ScienceDirect

Quaternary Science Reviews

journal homepage: www.elsevier.com/locate/quascirev

Local summer insolation and greenhouse gas forcing drove warming and glacier retreat in New Zealand during the Holocene

Lisa Dowling [a, b, *], Shaun Eaves [a, b], Kevin Norton [b], Andrew Mackintosh [c], Brian Anderson [a], Alan Hidy [d], Andrew Lorrey [e], Lauren Vargo [a], Matthew Ryan [b], Stephen Tims [f]

[a] Antarctic Research Centre, Victoria University of Wellington, PO Box 600, Wellington, 6140, New Zealand
[b] School of Geography, Environment and Earth Sciences, Victoria University of Wellington, PO Box 600, Wellington, 6140, New Zealand
[c] School of Earth, Atmosphere and Environment, Monash University, Melbourne, VIC, 3800, Australia
[d] Lawrence Livermore National Laboratory, Livermore, CA, USA
[e] National Institute of Water and Atmospheric Research, New Zealand
[f] Department of Nuclear Physics, Research School of Physics and Engineering, Australian National University, Canberra, ACT, 2601, Australia

ARTICLE INFO

Article history:
Received 10 January 2021
Received in revised form
14 June 2021
Accepted 24 June 2021
Available online 19 July 2021

Handling Editor: C. O'Cofaigh
Holocene
Glaciation
Southern Ocean
New Zealand
Cosmogenic surface exposure dating
Geomorphology
Glacial
Paleoclimate modeling
Southern Hemisphere
Little Ice Age
Moraine chronology

ABSTRACT

Geological climate archives from the Holocene Epoch provide baseline information concerning natural climate variability. Temperate mountain glacier extent is sensitive to summer air temperature, thus geological records of past glacier length changes are a useful proxy for this climatic variable. Here we present a new cosmogenic ^{10}Be chronology of glacier length changes at Dart Glacier in the Southern Alps, New Zealand. Prominent moraines deposited 321 ± 44 yr ago (n = 11) and 7.8 ± 0.3 ka (n = 5) show glaciers during the Little Ice Age were less extensive than during the early Holocene. This pattern of net Holocene glacier retreat is consistent with emerging data from other catchments in New Zealand and across the southern mid-latitudes. Using the physical framework of a transient global climate model simulation, we suggest that cool summers in the early Holocene were promoted by the local summer insolation minimum, together with low atmospheric greenhouse gas concentrations, causing an early Holocene austral glacial maximum. An insolation-driven reduction in seasonality at southern mid-latitudes may reconcile differences between early Holocene temperature reconstructions where climate proxies have different seasonal sensitivities. We suggest that rising greenhouse gas concentrations after 7 ka caused regional-scale glacier retreat and appear to be the dominant driver of multi-millennial summer temperature trends in the southern mid-latitudes during the present interglacial.

1. Introduction

Deconvolving natural drivers of climate variability from anthropogenic influences is a fundamental goal of climatological research. Successful detection and attribution of human influence in the climate system requires greater understanding of how and why climate has varied naturally during pre-industrial times. However, such understanding is limited by short instrumental records, especially in the Southern Hemisphere (Jones et al., 2016).

Glaciers are exceptional recorders of climate as their mass balance and length changes are strongly dependent on changes in temperature and precipitation (Oerlemans, 2001). Pre-historic glacier fluctuations are recorded in moraines, which delineate former ice geometries and record past glacier-climate interactions (Mackintosh et al., 2017b). Cosmogenic ^{10}Be surface exposure dating is an effective tool for accurately dating moraines (Balco, 2020). Developments in accelerator mass spectrometry (AMS) have allowed for samples collected from very young landforms (<1000 years old) with low ^{10}Be concentrations to be measured (Schaefer et al., 2009; Schimmelpfennig et al., 2014). Establishing secure chronologies of recent glacier change using cosmogenic ^{10}Be can thus extend historical climate records into the pre-industrial era and augment observational records.

New Zealand is an excellent location for glacier-climate reconstructions. The landmass is advantageously situated to record changes to the prevailing westerly circulation in the Southern

* Corresponding author. GNS Science, PO Box 30368, Lower Hutt, New Zealand.
E-mail address: l.dowling@gns.cri.nz (L. Dowling).

https://doi.org/10.1016/j.quascirev.2021.107068
0277-3791/

Hemisphere mid-latitudes (Lorrey and Bostock, 2017). Furthermore, steep topography coupled with the temperate, maritime, high-precipitation setting means that local glaciers are highly sensitive to changes in atmospheric temperature (Oerlemans and Fortuin, 1992; Mackintosh et al., 2017a, 2017b). To-date only a small number of Holocene cosmogenic moraine chronologies have been documented in New Zealand (Schaefer et al., 2009; Putnam et al., 2012; Kaplan et al., 2013; Eaves et al., 2019). Most of these glacier-climate reconstructions have been carried out in the central Southern Alps. Accurate constraints on the timing and magnitude of the climatic changes from geological records of past glacier length fluctuations require a dense population of Holocene moraine chronologies across a range of New Zealand sites.

In this study, we target a well-preserved moraine sequence at Dart Glacier (Fig. 1). We apply detailed geomorphological mapping and cosmogenic ^{10}Be surface exposure dating to reconstruct the pattern of glacier length changes at Dart Glacier and connect these observations with a rich observational record covering the last century. Finally, we integrate our data with previous geological data and examine the likely drivers of regional glacier length changes using the framework of a global climate model.

2. Study site

Dart Glacier (−44.37, 168.71) is a c. 7.6 km^2 valley glacier situated in the Mt. Aspiring/Tititea region of the Southern Alps/Kā Tiritiri o te Moana (Fig. 1) – currently the southernmost centre of glaciation in New Zealand (Baumann et al., 2020). The dominant lithology in the surrounding region is a psammitic greyschist of the Rakaia Terrane (Turnbull, 2000). The south-facing glacier descends from the highest peaks of the Snowdrift Range, 2400–2500 m above sea level (asl), forming the headwaters of the Dart River/Te Awa Whakatipu, which drains into Lake Wakatipu. The lake occupies a glacial trough excavated during Quaternary glacial cycles, when Dart Glacier was ~130 km longer than present (Barrell, 2011). Today the ~6 km-long glacier has a wide accumulation zone that becomes constricted at c. 1500 m asl, where an ice fall feeds the lower glacier tongue (Fig. 1), which terminates c. 1150 m asl (Fig. 2). Glacier modelling studies suggest that glaciers with this type of geometry have large length sensitivities compared to those with more uniform area-altitude distributions (Oerlemans, 2001). Dart Glacier also receives high amounts of precipitation (~5 m annually; Tait et al., 2006), which further enhances glacier sensitivity to temperature change (Oerlemans and Fortuin, 1992).

Dart Glacier has a detailed observational record extending through most of the 20th Century, which is rare for a glacier in the Southern Hemisphere. A surveying expedition in 1914 CE produced photographs and the first map of the region, published in 1915 CE (Wright, 1921). Subsequent observations from throughout the 20th Century (compiled by Bishop and Forsyth (1988) and Ruddell (1995)), show that Dart Glacier has retreated ~3 km from its historical 1915 CE terminus position to its 2018 CE terminus position (Fig. 2).

In addition to direct observations, a moraine record is preserved on the glacier foreland, extending ~8 km downstream from the present glacier terminus, which constrains pre-historic changes in ice surface height and glacier length. Sommerville et al. (1982) documented the biological succession and lichen (*R.Geographicum*) diameters across eleven bedrock and sediment ridges in two vertical transects on the eastern valley side: an 'upper site' between Dart Glacier surface and Cascade Saddle, and a 'lower site' approximately 5 km down-valley (Figs. 1 and 2). At ~1450 m asl, approximately 300 m above the present ice surface, there is a prominent, bouldery moraine ridge that Sommerville et al. (1982) labelled as 'U8' (Fig. 1) and attributed a lichenometry age of ~1850 CE. A similar age (~1837 CE) was derived for the morphological correlative of U8, labelled L8, at the lower transect site that is separated by a large landslide. Lichen measurements on the higher-elevation moraines (U/L9-11) indicated that the full sequence may represent glacier fluctuations since approximately 1750 CE. For consistency and ease of comparison, in this study we retain the landform labels as those used by Sommerville et al. (1982) (see Fig. 1B).

The findings of Sommerville et al. (1982) need to be reevaluated

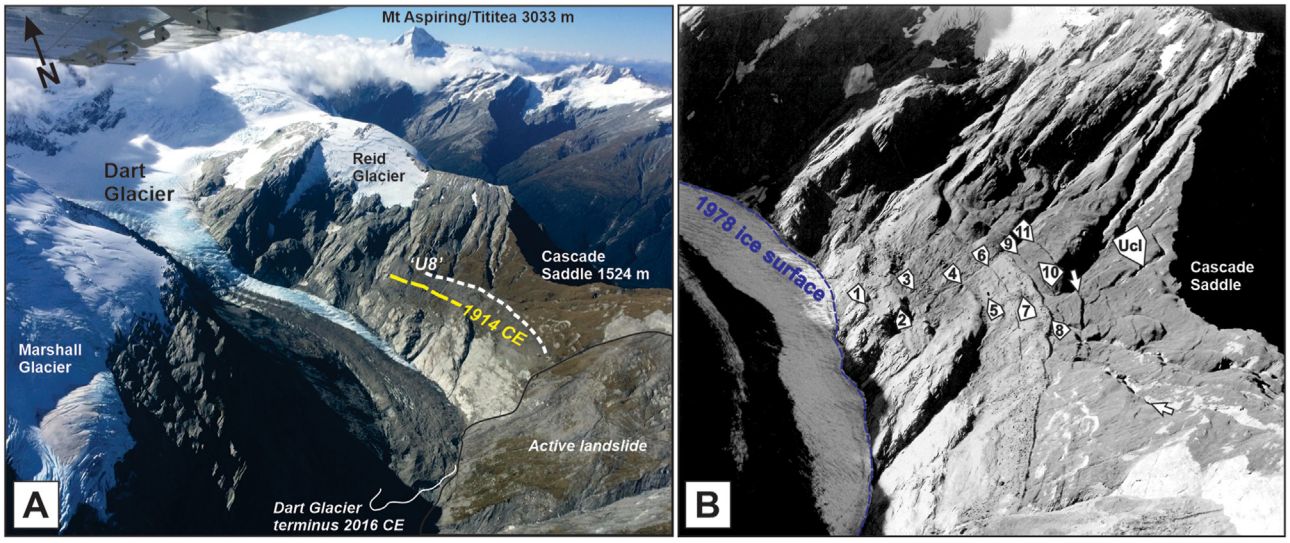

Fig. 1. *(a)* Annotated oblique aerial photograph of Dart Glacier taken in 2016 including the 'upper site' for ^{10}Be surface exposure dating of moraines in this study. On the eastern valley wall, outboard of ice sculpted bedrock, there is an area covered in glacier derived sediment including three prominent moraine ridges. Notably a prominent, bouldery moraine (U8), attributed a minimum lichenometry age of ~1850 CE by Sommerville et al. (1982), is delineated (white dashed line). The 1914 CE glacier position (yellow dash) is reconstructed from historical photos (Wright, 1921) that was verified during our field work. Vegetation at high-elevation on the valley side likely indicate areas that have not been recently glaciated. (B) The Cascade Saddle region depicted in low light showing the linear landforms recognised by Sommerville et al. (1982), which are labelled. White arrows illustrate continuously traceable bedrock surface that has moraine-like appearance at upstream end (Image credit: D.L. Homer/GNS Science). (For interpretation of the references to colour in this figure legend, the reader is referred to the Web version of this article.)

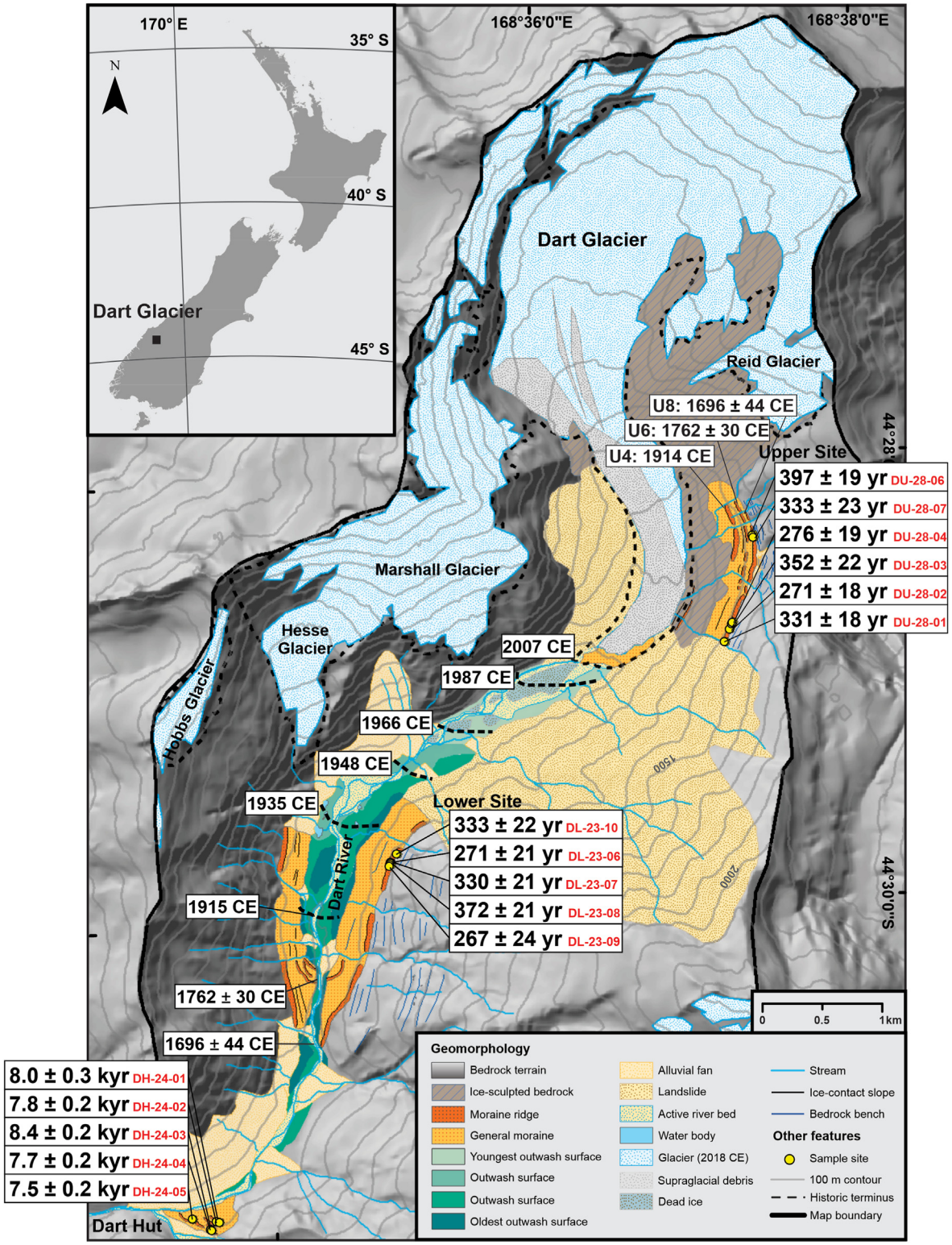

Fig. 2. Geomorphological map of the Dart Glacier foreland. Also shown are historic terminus positions as compiled by Bishop and Forsyth (1988), which are combined with the new ^{10}Be surface exposure ages from our study (yellow dots and associated labels). The 'upper' and 'lower' sites (labelled) broadly correspond to the locations of the two vegetation transects of Sommerville et al. (1982). The 1914 CE (U4) and 1762 ± 30 CE (U6) moraine ages are inferred from historical photographs and a recalibrated lichen growth curve, respectively. The U8 moraine arithmetic mean age of 1696 ± 44 CE is also included for context. Where lateral moraines converge on the valley floor at the lower site, we infer the age (1762 ± 30 CE) that correlates with the upper site U6 moraine age. Detailed views of the geomorphology mapped at the upper and lower sites (including sample locations from the U8/DU, L8/DL, and DH moraines) are included in Supplementary File. (For interpretation of the references to colour in this figure legend, the reader is referred to the Web version of this article.)

for several reasons. First, the ages derived by lichenometry use a lichen growth curve that was calibrated on late Holocene moraines at Lyell and Ramsay Glaciers (Burrows and Maunder, 1975), some 220 km northeast and 400–500 m lower in elevation than Dart Glacier. The uncertainty imparted by this geographic separation may be considerable. Second, the origin of some of the features identified by Sommerville et al. (1982) for determining the glacier history is unresolved. Sommerville et al. (1982) refer to all features as moraines, but later describe some as bedrock benches, which have unclear relationships to the glacier geometry. In this study we test these initial interpretations using detailed geomorphological field mapping, and ^{10}Be surface exposure dating, in order to construct a robust glacier length history that better facilitates interpretation of the associated climatic drivers.

3. Methods

3.1. Geomorphological mapping

We followed the approach of Barrell et al. (2011) to create a geomorphological map of the upper Dart valley that is comparable with other glacial geomorphological maps in the Southern Alps. Landforms were initially interpreted using vertical aerial photographs (Otago 0.75m Rural Aerial Photos, 2004–2011 and Otago 0.3m Rural Aerial Photos, 2017–2019), topographic base maps (NZ Topo50 series) and an 8 m digital elevation model (DEM) (https://data.linz.govt.nz/). Geomorphological interpretations were refined using field investigations, precise Global Navigation Satellite System (GNSS) data, and historical photographs and maps. Landforms were digitised using ArcGIS software and are displayed in the geomorphological map at 1:25,000 scale using the New Zealand Transverse Mercator (NZTM) projection.

3.2. Cosmogenic ^{10}Be surface exposure dating

3.2.1. Sample collection

We sampled sixteen schistose boulders situated on moraines in the upper Dart valley for cosmogenic ^{10}Be surface exposure dating (Table 1 & Fig. 2). The prominent moraine ridges in the upper Dart valley, previously labelled U8 and L8 (Sommerville et al., 1982), were targeted for sampling to determine whether these landforms formed contemporaneously or represent two distinct moraines with independent ages. In this study we label these samples with the prefix 'DU' and 'DL', respectively. To constrain the timing of an earlier glacier advance in the Dart valley, we collected samples from previously undescribed moraines identified during field mapping in the vicinity of Dart Hut, situated ~10 km from the present-day glacier terminus. In this study, these samples are labelled with the prefix 'DH'.

Application of cosmogenic surface exposure dating to moraines is subject to several assumptions that primarily concern the pre-depositional nuclide inventory and the post-depositional stability of the samples. We adhered to a sample-collection strategy designed to minimise violation of these assumptions. We targeted large boulders embedded in the crests of moraines, far from active geomorphic features, to minimise the likelihood of post-depositional boulder movement or erosion. We preferentially selected boulders with flat-topped surfaces, and minimal signs of weathering or sediment and vegetation cover to ensure that sampled surfaces have not been subject to erosion or burial (Fig. 3). Striated boulders would be desirable, as these features provide evidence of subglacial/englacial erosion and thus removal of any inherited ^{10}Be. However, we observed no obvious striae among the foliations of these schistose boulders. Quartz veins situated on the boulder surfaces were sampled using a hammer and chisel. At each sample site we measured boulder dimensions and documented the geomorphic context and boulder appearance (e.g. evidence of weathering). To determine topographic shielding of incoming cosmic rays, we surveyed the angle of the surrounding skyline using a clinometer and compass, along with the strike and dip of each sample surface. We recorded the location (latitude and longitude) and elevations of each sample using either a Trimble GeoXH or Garmin eTrex device (relative to WGS84 datum) (Table 1).

3.2.2. Sample preparation, sample measurement, and exposure age calculation

The moraine samples were processed in the Victoria University of Wellington (VUW) Cosmogenic Nuclide Laboratory following standard laboratory procedures for quartz separation and purification, and ^{10}Be extraction (Jones et al., 2015).

^{10}Be/^{9}Be ratios (Table 1) were measured at the Center for Accelerator Mass Spectrometry (CAMS) Lawrence Livermore National Laboratory (LLNL) relative to the 07KNSTD3110 standard (Nishiizumi et al., 2007). ^{10}Be/^{9}Be ratios were reduced using the protocol outlined by Balco (2006), which includes propagation of analytical, blank, and carrier uncertainties to the final ^{10}Be concentrations (Balco, 2006).

Surface exposure ages were calculated using version 3 of the online exposure age calculator formerly known as the CRONUS-Earth online exposure age calculator (https://hess.ess.washington.edu/). We used the 'Macaulay' *in situ* ^{10}Be production rate calibration dataset from the central Southern Alps established by Putnam et al. (2010). This production rate was favoured for the following reasons: (i) the regional proximity of the calibration site to Dart Glacier; (ii) the direct, independent radiocarbon ages for the Macaulay debris flow provide precise age constraint of the regional production rate; and (iii) the calibration site integrates cosmogenic ^{10}Be production over the Holocene, which is consistent with our application of surface exposure dating at Dart Glacier. Comparison of exposure ages calculated via a range of methods shows that the choice of production rate scaling scheme or production rate calibration dataset (i.e. local vs. global) does not influence the conclusions that are drawn from the calculated ages (Table 3). Hereafter, surface exposure ages are discussed using the 'Lm' scaling scheme (Balco et al., 2008) and 'Macaulay' production rate calibration (Putnam et al., 2010). Furthermore, we make no corrections for boulder surface erosion in our surface exposure age calculations as we targeted quartz veins that were elevated above the rock surface, indicating that the sampled surfaces have be subject to minimal erosion since exposure. However, even in the extreme case that the erosion rate is 5 mm/kyr, the calculated exposure ages increase by 5–9%. Such an increase in surface exposure ages does not have a significant impact on our conclusions.

4. Results

On the eastern valley side, immediately outboard of the present-day ice surface, we identified ice-sculpted bedrock that comprises glacially-polished and striated (oriented parallel to the current ice flow direction) upstream faces, and steep jagged downstream slopes (Fig. 2). Much of this terrain has become exposed by glacier thinning during the 20th Century (Fig. 1; Bishop and Forsyth, 1988). Further upslope, we distinguished three well-defined moraine ridges on the eastern valley wall that are surrounded by general moraine (Fig. 2). The two innermost moraine ridges, situated at ~1370 m asl and ~1410 m asl, are semi-continuous discrete ridges comprising glaciogenic sediment, however, no suitable boulders for cosmogenic ^{10}Be surface exposure dating were identified on the

Table 1
$^{10}Be/^{9}Be$ ratios and ^{10}Be concentrations and all information associated with analysis and exposure age calculations for samples collected from the upper, lower and Dart Hut study sites. Exposure ages were also calculated with a sample density of 2.7 g cm^{-3}, erosion rate of 0 cm yr^{-1}, elevation flag 'std' and AMS standard 07KNSTD (Nishiizumi et al., 2007).

Sample ID	Latitude (DD)	Longitude (DD)	Elevation (m asl)	Boulder size (L × W × H) (cm)	Sample thickness (cm)	Topographic shielding correction	Quartz mass (g)	^{9}Be mass (μg)	$^{10}Be/^{9}Be \pm 1\sigma$ (10^{-14})	^{10}Be conc. $\pm 1\sigma$ (10^{3} at g^{-1})	Blank
Upper Site (DU/U8) Moraine											
DU-28-01	−44.48045	168.61706	1431	370 × 200 × 140	3	0.9748	74.2451	273	2.467 ± 0.077	4.501 ± 0.246	Blank 3
DU-28-02	−44.47954	168.61768	1426	340 × 290 × 130	2	0.9789	73.1789	273	2.128 ± 0.078	3.723 ± 0.243	Blank 3
DU-28-03	−44.47915	168.61793	1427	180 × 110 × 70	2	0.9670	69.2093	272	2.452 ± 0.092	4.767 ± 0.293	Blank 3
DU-28-04	−44.47904	168.61802	1427	490 × 490 × 390	3	0.9764	77.2822	272	2.438 ± 0.088	3.750 ± 0.264	Blank 1
DU-28-06	−44.47259	168.62057	1447	680 × 280 × 240	3	0.9817	78.0012	273	2.987 ± 0.084	5.498 ± 0.258	Blank 3
DU-28-07	−44.47273	168.62064	1450	540 × 410 × 440	4	0.9794	71.7793	273	2.434 ± 0.011	4.576 ± 0.314	Blank 3
Lower Site (DL/L8) Moraine											
DL-23-06	−44.49569	168.58084	1215	170 × 110 × 50	2	0.9523	74.2860	273	1.884 ± 0.081	3.071 ± 0.243	Blank 3
DL-23-07	−44.49575	168.58081	1219	90 × 68 × 80	2	0.9510	71.6424	273	2.103 ± 0.070	3.740 ± 0.233	Blank 3
DL-23-08	−44.49580	168.58076	1213	280 × 180 95	1.5	0.9286	73.4435	273	2.287 ± 0.073	4.106 ± 0.236	Blank 3
DL-23-09	−44.49582	168.58081	1215	240 × 85 × 90	2.5	0.9624	75.0164	272	2.094 ± 0.092	3.036 ± 0.274	Blank 1
DL-23-10	−44.49489	168.58125	1213	265 × 120 × 120	2	0.9701	70.2485	273	2.109 ± 0.076	3.828 ± 0.250	Blank 3
Dart Hut (DH) Moraines											
DH-24-01	−44.52188	168.56055	995	340 × 220 × 82	2	0.9513	61.7795	273	24.53 ± 0.66	70.143 ± 2.397	Blank 5
DH-24-02	−44.52197	168.56087	996	670 × 215 × 200	2.5	0.9619	73.8690	272	28.87 ± 0.53	68.883 ± 1.883	Blank 1
DH-24-03	−44.52247	168.55989	998	435 × 150 × 120	2.5	0.9647	66.0162	272	27.91 ± 0.52	74.526 ± 2.058	Blank 1
DH-24-04	−44.52254	168.55997	998	260 × 170 × 60	3	0.9589	74.7486	272	28.69 ± 0.53	67.731 ± 1.868	Blank 1
DH-24-05	−44.52160	168.55806	974	790 × 420 × 430	1.5	0.9581	61.6865	272	22.87 ± 0.43	65.253 ± 1.809	Blank 5

Table 2
Process blank $^{10}Be/^{9}Be$ ratios and ^{10}Be atom totals.

Sample ID	^{9}Be mass (μg)	$^{10}Be/^{9}Be \pm 1\sigma$ (10^{-15})	$^{10}Be \pm 1\sigma$ (10^{5}at)
Blank 1	271.755	8.444 ± 0.492	1.533 ± 0.094
Blank 3	272.609	6.350 ± 0.409	1.157 ± 0.078
Blank 5	272.457	7.554 ± 0.503	1.375 ± 0.095

crests of these moraines. At approximately 1440 m asl, we identified the U8 moraine also identified by Sommerville et al. (1982) (Fig. 2). This feature is the most distinctive of the three moraine ridges in the upper site with large boulders (Table 1) well embedded in the moraine crest (Fig. 4A). We sampled six of these boulders for cosmogenic ^{10}Be surface exposure dating, which yielded ages 271 ± 18 yr to 397 ± 19 yr (Fig. 2 and Table 3). The ice-distal side of the moraine ridge is steep and rises ~1 m above the valley wall. This moraine is the most continuous of the three identified in the upper study site, extending ~1.2 km down valley to where it is dissected by a stream and large landslide deposit (approximately 3 km wide) (Fig. 2).

We inspected the composition of the three moraine ridges situated outboard of the U8 moraine (U9-U11; Fig. 1) identified by Sommerville et al. (1982). While these ridges are morphologically similar and sub-parallel to the U8 moraine, they are almost entirely devoid of surface boulders. Examining the deep gullies where these features have been incised into by streams, we found that these ridges comprise a bedrock core that extends almost to the surface, where it is mantled by thin soil and surface vegetation. Furthermore, these ridges can be traced near-continuously across the drainage divide to the eastern slopes of Cascade Saddle (Figs. 1B and 4A), indicating a structural control. At this location, the schist bedrock dips steeply (25–40°) and strikes broadly north-south (Turnbull, 2000), which is sub-parallel with the valley axis of the Dart Glacier proglacial region forming a geomorphic dip slope (Fig. 4A). Thus, based on our field study we do not recognise these features as moraine ridges. Instead we interpret these features as structurally-controlled linear bedrock benches. While it is probable that parts of the hillslope above the U8 moraine have been ice-covered in the past, for example during construction of the DH moraines (Fig. 2), we do not recognise any clear constructional glacial landforms indicative of former stable ice margins.

At the lower site on the eastern valley wall, the L8 moraine has similar glacial geomorphology to that described for the upper site (Fig. 4B). The moraine is located approximately 200 m above the valley floor at ~1200 m asl (Fig. 2). The well-defined ridge can be traced for ~2 km despite minor dissection by stream incision and is cut at the northern end by the same landslide deposit that cuts the southern section of the upper site moraine sequence. Boulders were found embedded in the crest of the moraine, 5 of which were sampled for cosmogenic ^{10}Be surface exposure dating. Exposure ages of these samples range from 271 ± 21 yr to 372 ± 21 yr (Table 3 and Fig. 5). A similar feature is mirrored on the western valley wall (Fig. 2), although this moraine ridge is less well preserved due to fluvial erosion and slope movement. These two prominent,

Fig. 3. Images of sampled boulders and their associated exposure ages and uncertainties (arithmetic mean ages and standard deviation values, respectively) and sample names.

outermost moraine ridges continue down valley gradually converging towards the valley floor, delineating the former shape of Dart Glacier when the terminus was situated at approximately ~1000 m asl and ~4.3 km down valley from the present-day glacier terminus. We also identified several smaller moraine ridges inside the described former glacier terminus (Fig. 4D), which likely correlate with moraines positioned inboard of the U8 moraine (e.g. U6), however, no boulders on these features were sampled for ^{10}Be surface exposure dating. Similar to the upper site, outboard of the outer moraine ridge (L8) on the eastern valley wall there are several discontinuous bedrock benches.

Further downstream, both east and west valley walls are heavily vegetated. In the vicinity of the Dart Hut, we identified a hummocky landform with abundant surface boulders situated above the main Dart valley floor (Fig. 2). Inaccessible sediment exposures on the Dart River side, observed from a distance, indicate that it comprises poorly sorted sediment with weak stratification, indicating depositional features as opposed to the erosional bedrock benches described earlier. The landform comprises a nested sequence of discrete ridges oriented parallel to subparallel with the valley axis and with abundant surface boulders (Fig. 4E). The surface of this deposit bears no evidence of post-depositional fluvial action (e.g. erosional escarpments, alluvial channels/plains between topographic highs) indicating that the continuous, bouldery ridges are primary, constructional features. Such organisation is consistent with that expected from lateral moraines and inconsistent with products of landslides which tend to be distributed more chaotically (McColl et al., 2019). Furthermore, the topographic situation of the landform does not support a mass movement origin. The landform is perched on the lower slopes of the spur descending westwards from Headlong Peak. The only hillslopes from which this material may have been sourced via mass movement are (i) the south-facing slope on the opposite side of the Dart River, and the heavily-vegetated north-facing slope immediately to the south, neither of which bear evidence for significant failure in the recent geological past. We thus interpret this landform as a sequence of nested lateral/latero-terminal moraine ridges deposited by a formerly extended Dart Glacier. We sampled five large boulders

Table 3
Cosmogenic ^{10}Be exposure ages for the moraines in the Dart valley calculated using the version 3 exposure age calculator (Balco, 2017). Ages are reported in years before 2017 CE with their internal uncertainty which accounts for all propagated uncertainties (analytical, blank and carrier) within the reported ^{10}Be concentration 1σ uncertainties (Table 2). Reported exposure ages were calculated using three scaling schemes: St (Stone, 2000), Lm (Balco et al., 2008), and LSD (Lifton et al., 2014) and using the 'Macaulay' production rate calibration dataset of Putnam et al. (2010). Ages calculated using the 'global' primary production rate calibration dataset of Borchers et al. (2016) are also reported for comparison. Arithmetic mean ages and standard deviations for each of the three landforms are reported, as well as the "pruned" summary ages (error-weighted mean and standard error; Balco, 2017). Italicised ages indicate outliers identified by the chi-squared test implemented in the online calculator, which are removed in the pruned summary ages. Note that we use the arithmetic mean ages (bold) in this study and no outliers were removed (see main text).

Sample ID	St age (yrs)	Lm age (yrs)	LSD age (yrs)	Lm age (yrs) (global)
Upper Site (DU/U8) Moraine				
DU-28-01	362 ± 20	331 ± 18	312 ± 17	315 ± 17
DU-28-02	297 ± 19	271 ± 18	260 ± 17	258 ± 17
DU-28-03	*384 ± 24*	*352 ± 22*	*330 ± 20*	*335 ± 21*
DU-28-04	302 ± 21	276 ± 19	264 ± 19	263 ± 18
DU-28-06	*434 ± 20*	*397 ± 19*	*372 ± 17*	*378 ± 18*
DU-28-07	364 ± 25	333 ± 23	313 ± 21	317 ± 22
Pruned age (n = 4; 2 outliers removed)	353 ± 36	323 ± 33	296 ± 32	307 ± 34
Arith. mean (n = 6)	**357 ± 52**	**327 ± 48**	**309 ± 42**	**311 ± 45**
Lower Site (DL/L8) Moraine				
DL-23-06	296 ± 23	271 ± 21	262 ± 21	258 ± 20
DL-23-07	360 ± 22	330 ± 21	314 ± 20	314 ± 20
DL-23-08	*405 ± 23*	*372 ± 21*	*352 ± 20*	*354 ± 20*
DL-23-09	291 ± 26	267 ± 24	258 ± 23	254 ± 23
DL-23-10	363 ± 24	333 ± 22	316 ± 21	317 ± 21
Pruned age (n = 4; 1 outlier removed)	328 ± 39	300 ± 36	290 ± 10	*286 ± 37*
Arith. mean (n = 5)	**343 ± 49**	**315 ± 45**	**300 ± 40**	**299 ± 44**
Dart Hut (DH) Moraines				
DH-24-01	8073 ± 277	7959 ± 273	7854 ± 269	7594 ± 260
DH-24-02	7868 ± 216	7766 ± 213	7670 ± 210	7410 ± 203
DH-24-03	8475 ± 235	8356 ± 231	8224 ± 228	7957 ± 220
DH-24-04	7779 ± 215	7681 ± 212	7590 ± 210	7327 ± 203
DH-24-05	7552 ± 210	7466 ± 208	7402 ± 206	7107 ± 198
Arith. mean (n = 5)	**7950 ± 348**	**7846 ± 336**	**7748 ± 312**	**7479 ± 319**

embedded in the crests of these prominent moraine ridges for cosmogenic ^{10}Be surface exposure dating. These exposure ages for these samples range from 7.5 ± 0.2 to 8.4 ± 0.2 yrs (Table 3 and Fig. 5).

5. Discussion

5.1. Moraine chronology

The individual moraine age datasets show good internal consistency (Table 3). We used a chi-squared outlier detection routine, as implemented in the version 3 exposure age calculator (Balco, 2017), to assess the significance of the spread in the ^{10}Be exposure ages for individual moraine datasets. This technique identifies two potential outliers within the DU moraine population (DU-28-03, DU-28-06) and one DL sample (DL-23-08). Each of these samples yields exposure ages that exceed the mean age of the moraine population, which indicates potential inheritance of ^{10}Be from a period of prior exposure. However, the amount of inheritance is low, on the order of decades, and removal of these ages has little impact on the mean moraine ages (Table 3). An alternative interpretation is that these oldest ages in the populations represent the true depositional age, and the remaining younger ages have been affected by post-depositional processes, such as erosion. Furthermore, it is noteworthy that both the U8 and L8 moraines exhibit bimodal distributions (Fig. 5A), which may be indicative of multiple moraine construction phases. Although, based on our field observations there is no evidence to suggest that this is a composite feature as all boulder samples were taken from a single, discrete, and continuous moraine crest. It is not possible to unambiguously resolve these competing explanations and the implications for the glacial history are negligible regardless of which is correct (e.g. Table 3). Thus, we take a conservative approach to moraine age and uncertainty calculation by retaining all samples and using the weighted arithmetic mean ages and their standard deviations (Table 3). Moraine ages for the upper and lower sites (U8 and L8) are 327 ± 48 yr and 315 ± 45 yr, respectively (Table 3). These populations are statistically indistinguishable at 1σ-level of uncertainty thus we are confident that these two moraine segments formed coevally and were once continuous prior to severance by the hillslope instability between our two sample locations (Fig. 2). Combining these ages yields a mean age for this landform of 321 ± 44 yr (Table 3; Fig. 5A).

When expressed as a calendar age, this result indicates that the moraine formed in 1696 ± 44 yr CE, which is ~150 yr earlier than the relative age indicated by lichenometry (Sommerville et al., 1982). Coexisting measurements of lichen diameters (in ~1982 CE) and ^{10}Be exposure ages at U8, coupled with direct glacier observations in 1914 CE at U4, allow for an age estimation of intermediate moraines with lichen measurements that remain undated by ^{10}Be (e.g. Putnam et al., 2012). We use linear interpolation with a Monte-Carlo based resampling approach for error propagation (see Supplementary Information) to estimate the age of the prominent U6 moraine, a bouldery moraine situated approximately 30 m below U8. This approach returns an age estimate of 1762 ± 30 CE (1 σ) (Fig. 5C).

At the lower most site targeted in this study, the five ages from moraine ridges close to Dart Hut yield no outliers (Table 3). The arithmetic mean and standard deviation of these coherent samples is 7.8 ± 0.3 ka (n = 5; 1σ) (Table 3; Fig. 5B).

Overall, our new ^{10}Be moraine chronology constrains the former ice geometry at 7.8 ± 0.3 ka and 321 ± 44 yr ago. Preservation of the older moraine indicates that Dart Glacier length has not exceeded this position since moraine formation and thus has undergone net retreat during the Holocene. Absence of moraines in the ~2 km that separate the features dated here, may represent a lack of

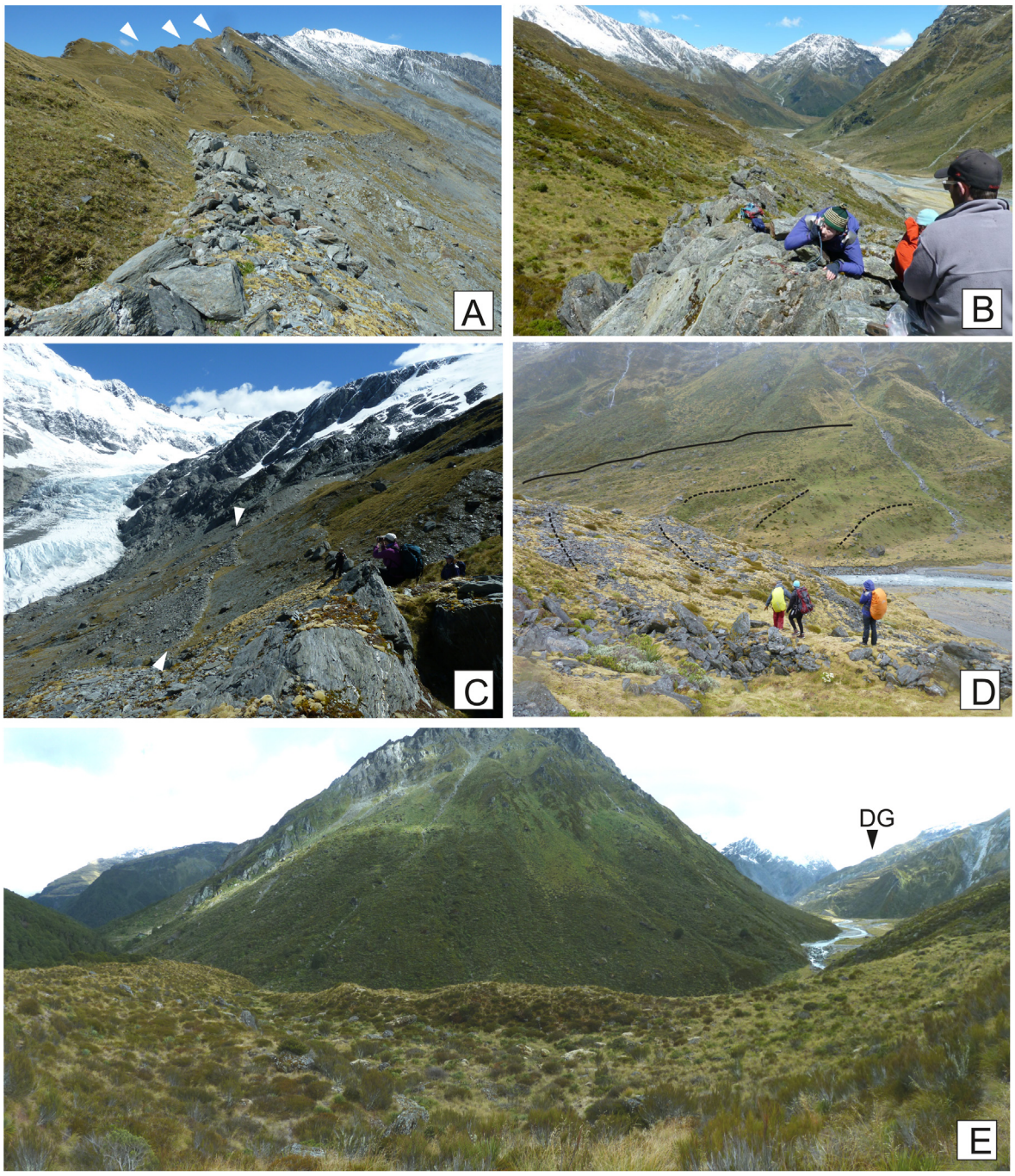

Fig. 4. Selected geomorphology of the upper Dart valley. (A) The prominent U8 moraine marks a clear vegetational break on the hillslope (view oriented down-valley). In the background, the structure of the underlying strata can be seen - white arrows illustrate the dip slope controlling the bedrock ridge forms seen in panel A. (B) The L8 left-lateral moraine pictured at our 'lower site'. (C) Looking up-glacier from the prominent U8 moraine, the U6 moraine (defined by Sommerville et al., 1982) is demarcated by the white triangle annotations. (D) Nested latero-terminal moraines are evident on both sides of the Dart River (delineated by thin dashed lines). On the far hillslope, the U8/L8 right lateral correlative can be seen projecting further down-valley (solid black line). (E) Panoramic photo of the nested DH moraines (up-valley (DG = Dart Glacier) is to the right, down-valley to the left). The prominent linear ridge (centre, foreground) is bound by a similar form from which the image was taken and can be seen at the left side of the image.

preservation, or indicate that Dart Glacier remained inside the 0.3 ka limit after 7.8 ka. The U8/L8 moraine, now dated to 1696 ± 44 CE, can be traced to the valley floor indicating that Dart Glacier was 10.5 km long at that time. Approximately 0.5 km up-valley from this former limit, there is a sequence of nested terminal moraines (Fig. 2; Fig. 4D), which we correlate to the prominent U6 moraine that we estimate formed in 1762 ± 30 CE (see above). Historical observations of Dart Glacier further capture the progressive ~3.5 km retreat of the glacier up the valley to its present-day terminus since ~1914 CE (Fig. 1, Bishop and Forsyth, 1988; Ruddell, 1995). Approximately two-thirds of the total 6.3 km glacier retreat that has taken place between 7.8 ka and present occurred after 1915 CE.

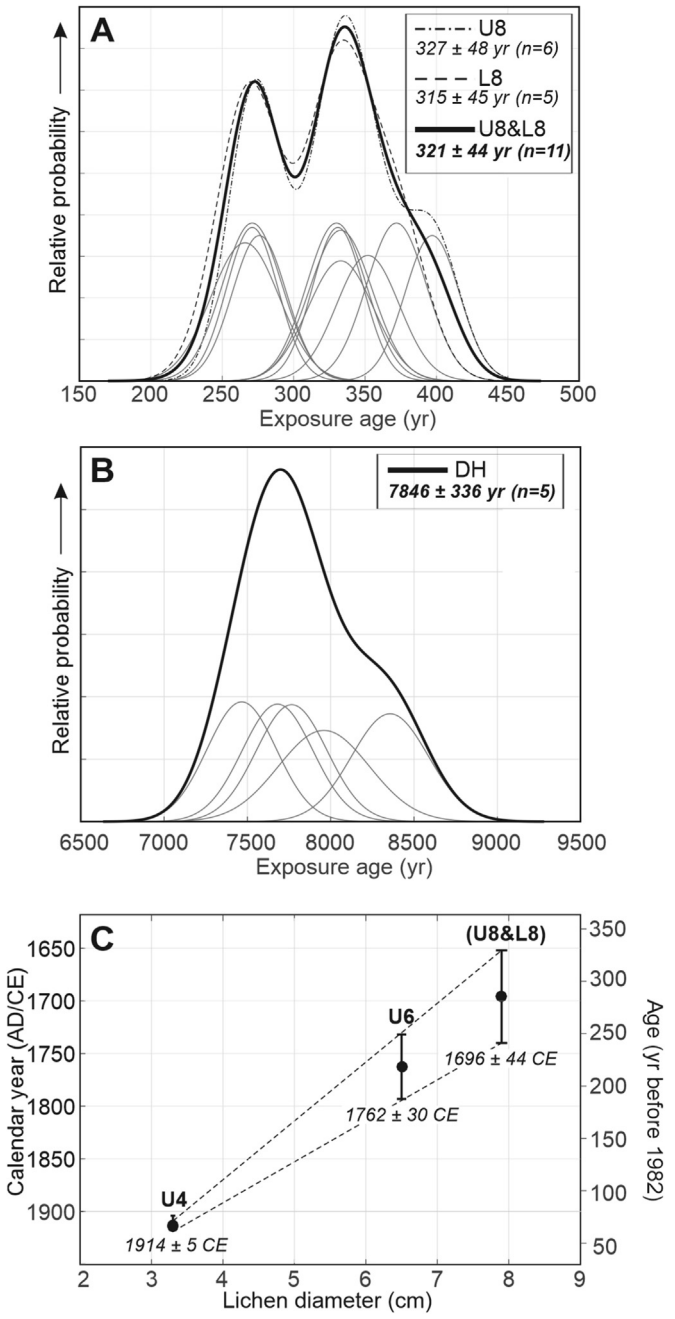

Fig. 5. Kernel density estimates (camelplots) of the ^{10}Be exposure ages from (A) the upper and lower sites (U8 and L8 of Sommerville et al. (1982), respectively) including combined (arithmetic mean) age for U8 and L8 moraines and (B) the Dart Hut (DH) moraines. (C) Construction of a local lichen growth curve calibration using the historical observations and our ^{10}Be data, from which an age estimate for the U6 moraine identified by Sommerville et al. (1982) (located in between the U4 and U8 moraines) is linearly interpolated.

5.2. Holocene glacier fluctuations in New Zealand

Combining the moraine record from Dart Glacier with those records from the central Southern Alps (Schaefer et al., 2009; Putnam et al., 2012; Kaplan et al., 2013; Winkler, 2014) provides a composite chronology of Southern Alps glacier fluctuations (n = 165 ^{10}Be ages) that can be used to assess whether glacier length changes in different mountain valley glaciers followed a broadly similar trend. Comparison between early Holocene ^{10}Be moraine records suggests that moraine formation occurred coevally at Dart Glacier, Whale Stream in Ben Ohau Range, and Cameron Glacier. Moraines also formed in the central Southern Alps prior to 7.8 ka (Fig. 6; Putnam et al., 2012; Kaplan et al., 2013), yet no moraines deposited during this time were observed in the Dart valley. It is possible that moraines were deposited in the Dart valley prior to 7.8 ka, though they may have been destroyed by post-depositional processes or obscured by the dense vegetation cover downstream of the Dart Hut site.

The composite moraine chronology for the Southern Alps (Fig. 6) shows that early Holocene glacier advances culminated in New Zealand between ~8 and 7 ka. This culmination immediately precedes a hiatus in the moraine record between ~7 and 3 ka. This gap may indicate a prolonged period of glacier retreat in the Southern Alps, during which time glaciers were at least shorter than during the late Holocene (post ~3 ka). Alternatively, the absence of mid-Holocene moraines in the regional compilation could be an artefact of sampling; that is, these moraines exist but have not been identified. For example, Eaves et al. (2019) identified a 4.5 ka moraine on Mt Ruapehu in central North Island, which indicates greater ice extent at that time than during the last millennium. Further sampling of moraines and glacially-eroded bedrock in New Zealand will help to elucidate the meaning of this gap in the composite moraine chronology for the Southern Alps (Fig. 6).

The 321 ± 44 yr old moraine at Dart Glacier formed at a similar time to other moraines in the Southern Alps. The most comparable moraine ages are reported at Mueller Glacier by Schaefer et al. (2009) at 311 ± 8 (n = 6) (Site Scha2009-C; recalculated using the same production rate and scaling scheme parameters as this study), although this moraine has been interpreted as a minor standstill or readvance that occurred after a larger advance denoted by the 577 ± 14 yrs (n = 7) moraine (Fig. 6A). Putnam et al. (2012) also suggest that the most significant glacier advance at Cameron Glacier during the last millennium occurred during the early 15th Century, which occurs within the timeframe of the Northern Hemisphere Little Ice Age (14th to 19th Century) (Fig. 6A). These ages contrast with the findings from Dart Glacier which show that the most significant late Holocene glacier advance occurred during the late 17th Century. Moraine chronologies from Cameron and Mueller glaciers show that glacier advance during the early 15th Century was followed by glacier retreat and several standstills or minor readvances at that occurred between the 15th and 20th centuries (Schaefer et al., 2009; Putnam et al., 2012) (Fig. 6A). Moraines formed during standstills or minor advances are also found at Dart Glacier inboard of the 321 ± 44 yr old moraine; recalculation of the lichenometry ages presented by Sommerville et al. (1982) and historical records suggest that these occurred at ~1760 CE and ~1914 CE. Previous palaeoclimate modelling and proxy synthesis work has indicated the 1450-1850 CE interval saw variable but overall cooler summer temperatures across the Southern Alps, likely driven by a combination of climate modes, with more frequent southerly and westerly flow over New Zealand (Lorrey et al., 2014).

Evidently, there is some overlap between the timing of moraine formation at Dart Glacier and other mountain glaciers in the central Southern Alps (Fig. 6). Differences between moraine preservation and the exact timing of moraine formation may reflect variations between individual glacier response times and length sensitivities (Mackintosh et al., 2017b), as well as chronological uncertainties. The geometry and climatic setting of Dart Glacier promotes a relatively short response time that causes the glacier to fluctuate regularly in response to both high-frequency (interannual to decadal) and low-frequency (multi-decadal to centennial) climate changes (Purdie et al., 2014; Mackintosh et al., 2017a, 2017b).

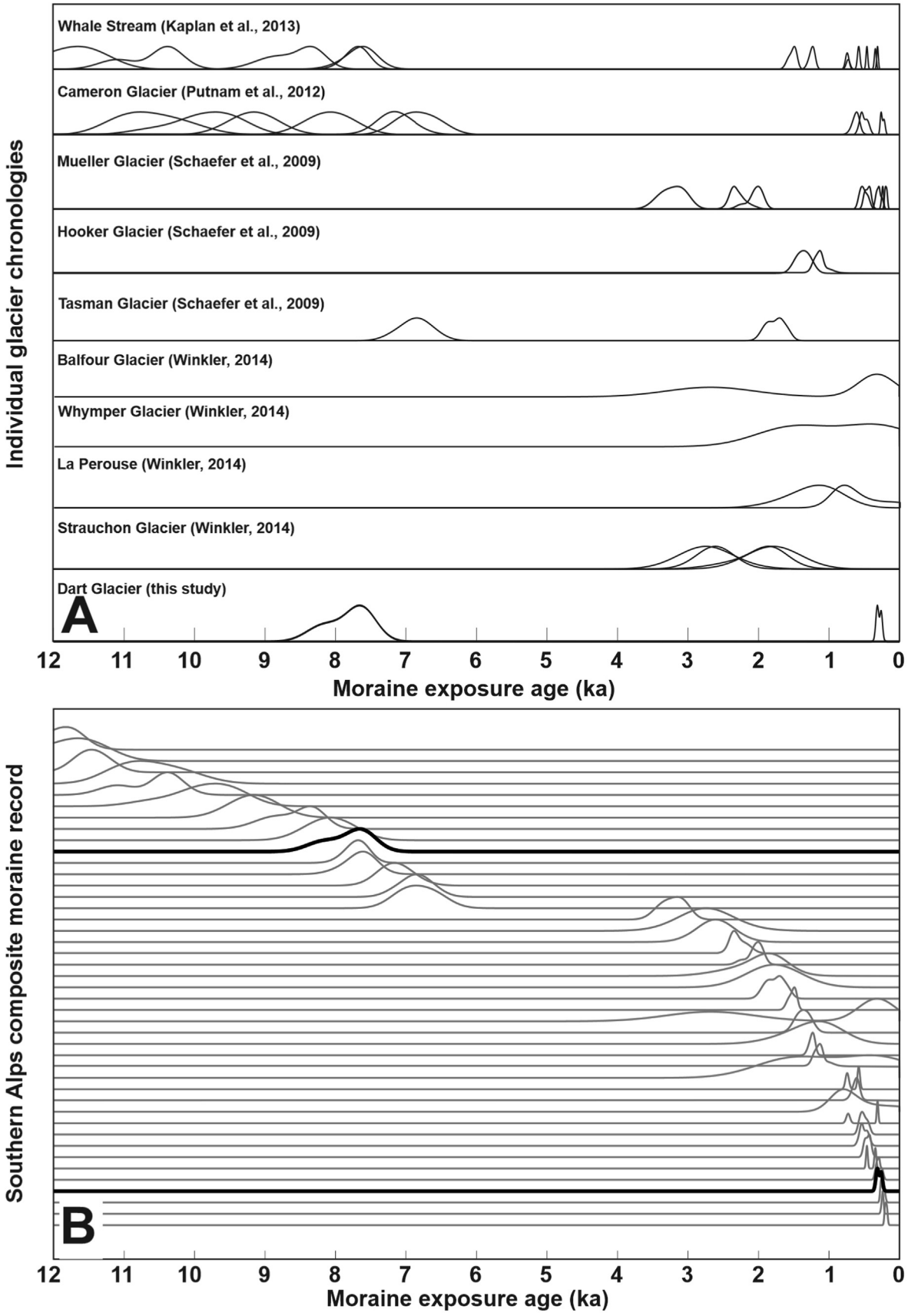

Fig. 6. Compilation of Holocene moraine records in the Southern Alps dated using cosmogenic ^{10}Be surface exposure dating. Kernel density estimates denote individual moraine exposure ages from different mountain valleys in the Southern Alps (A). Individual moraine chronologies are stacked and organised chronologically to form a composite moraine

Evidence of Dart Glacier's relatively short response time is shown by the clear moraine formed in ~2010 CE (Fig. 2) during the short-lived advance phase of New Zealand glaciers (Mackintosh et al., 2017a).

Several glaciers in other adjacent mountain valleys, such as Mueller Glacier, would be expected to have comparatively longer response times and lower length sensitivities because of their gentle bed slopes, high percentage of surface debris cover, and geometries which consist of small, confined accumulation zones and widening ablation zones (Schaefer et al., 2009; Mackintosh et al., 2017b). While the Southern Alps glaciers were likely forced by the same climate signals in the past, several of these glaciers fluctuate less frequently in response to climate perturbations and therefore exhibit more compound moraine sequences (e.g. Mueller and Cameron glaciers) (Mackintosh et al., 2017b). In contrast, Dart Glacier may experience more frequent fluctuations compared to adjacent valley glaciers. Furthermore, in the Dart Glacier valley, meltwater systems, aggrading outwash surfaces, mass movement, and steep terrain may have impacted moraine preservation.

5.3. Climatic drivers of observed glacier trends

The composite Southern Alps moraine record presented in Fig. 6, including the ~7.8 ka ^{10}Be moraine age at Dart Glacier, indicates multiple episodes of moraine formation between ~12 and 7 ka. Preservation of these features suggests that New Zealand glaciers were larger during the early Holocene than at any other time in the Holocene Epoch.

The apparent early Holocene glacial maximum conflicts with numerous regional marine and terrestrial palaeoclimate records that suggest warmer-than-present sea-surface and air temperatures at this time (e.g. Masson et al., 2000; Wilmshurst et al., 2007; Marcott et al., 2013; Prebble et al., 2017). However, multi-proxy analyses of ecological climate indicators with contrasting seasonal sensitivities suggest that the early Holocene in New Zealand was characterised by lower seasonality (cooler summers, warmer winters) than present (McGlone et al., 2010b; van den Bos et al., 2018; Lorrey et al., 2020). Glacier modelling studies have highlighted that mountain glacier mass balance is more sensitive to summer temperature change (Oerlemans and Reichert, 2000). Thus, preservation of early Holocene moraines at Dart Glacier, and elsewhere in the Southern Alps, is consistent with New Zealand proxy evidence that indicates low seasonality and cooler summer temperatures relative to present-day (e.g. McGlone et al., 2010a; McGlone et al., 2010b; Putnam et al., 2012; Kaplan et al., 2013; van den Bos et al., 2018).

Looking further afield to southern South America there is a lower density of glacier chronologies compared to the Southern Alps, meanwhile current records suggest some heterogeneity in Holocene glacier trends. Existing evidence indicates a prominent period of glacier advance during the mid-Holocene (c. 7–4 ka; Menounos et al., 2013; Kaplan et al., 2016; Reynhout et al., 2019), which coincides with the apparent hiatus in moraine deposition in New Zealand. Evidence to constrain early Holocene glacier extent is more lacking. Some studies have noted evidence for a period of glacier contraction at this time (Strelin et al., 2014; Hall et al., 2019), however at other locations evidence exists for glacier advances of greater extent than the mid and late Holocene (Wenzens, 1999; Douglass et al., 2005; Harrison et al., 2012). Several previous authors have noted the challenge of deriving composite regional climate records from Patagonian glacier chronologies (Harrison et al., 2012; Reynhout et al., 2019), which often comprise indirect radiocarbon ages often from complex outlet glaciers and/or tidewater settings.

Recent studies have demonstrated similar Holocene glacier trends to those in the Southern Alps. Reynhout et al. (2019) document that the largest Holocene advance at Glaciar Torre culminated at 9.7 ± 0.4 ka, followed less extensive advances during the mid and late Holocene. Offshore, Bakke et al. (2021) report a pattern of glacier change on South Georgia that is very similar in nature to the composite Southern Alps record, with millennial-scale moraine-forming events between 9 ka and present, superimposed on an overall trend of declining glacier length. These records are notable as they comprise comparable methods (^{10}Be exposure dating) applied to similar glacial settings to those in the Southern Alps, i.e. moraines deposited by small, land-terminating alpine glaciers of relatively simple geometry. Emergence of these records may challenge previous suggestions of pronounced asymmetry in Holocene climate trends derived from existing glacier chronologies. Overall, we echo Hall et al. (2019) who call for a greater focus on terrestrial glacier records to help resolve the Holocene glacier and climate trends in southern South America.

To better understand the possible role of large-scale drivers of Holocene glacier and climate change trends in the New Zealand region, we examine outputs from the Transient simulation of Climatic Evolution of the last 21,000 years (TraCE-21k) experiments undertaken using Community Climate System Model (version 3; CCSM3; data available: https://www.earthsystemgrid.org/project/trace.html). The TraCE-21ka experiments include transient simulations of the Holocene undertaken using fully-coupled atmosphere-ocean models (He, 2011). We extracted seasonal 2-m air temperature in the Southern Alps from the suite of sensitivity experiments that simulate the climatic response to orbital forcing (ORB), greenhouse gases (GHG), meltwater forcing (MWF), and changing ice sheet geometry (ICE), as well as their combined influence (ALL) (Fig. 7).

Under the ALL-forcings scenario, there is a clear difference in the seasonal evolution of temperature anomalies in the Southern Alps (Fig. 7). In the early Holocene (c. 10–8 ka), winter (June–August) air temperatures are close to pre-industrial (~1850 CE) values, whereas summer (December–February) air temperatures are more than half a degree (−0.63 °C) cooler than pre-industrial. Reduced seasonality at the onset of the interglacial is consistent with larger glaciers (Fig. 6) as well as other local proxy data that indicates mild winters and cool summers (e.g. McGlone et al., 2010b; van den Bos et al., 2018; Lorrey et al., 2020).

Looking to the sensitivity runs (Fig. 7, panels b–e), only orbital forcing produces a markedly different seasonal response (Fig. 7b). However, the magnitude of the seasonality reduction in the ORB experiment is only one-third of that seen in the ALL-forcings simulation, which suggests that some feedbacks must be responsible for amplifying the effects of insolation in the early Holocene. A similar impact is seen in the meltwater (MWF) experiment where a large temperature spike at 8 ka, probably reflecting the mechanisms outlined by Pedro et al. (2018), is not manifested in the ALL-forcings simulation due to the warming effects of the other forcings that have dampened any potential feedbacks.

The largest impact on summer temperatures, which appears to be persistent between the ALL-forcings simulation and the sensitivity experiment, is imparted by greenhouse gas changes (GHG), of which carbon dioxide dominates (Joos and Spahni, 2008). In the GHG simulation, summer air temperatures in New Zealand

record for the Southern Alps (B). The two Dart moraines are highlighted (bold) at 7846 ± 336 yrs and 321 ± 44 yrs. All ^{10}Be surface exposure ages were calculated using the same parameters as this study and cosmogenic nuclide measurements from the Alpine-ICE-D database (http://alpine.ice-d.org/) Figure produced using code originally constructed by G. Balco.

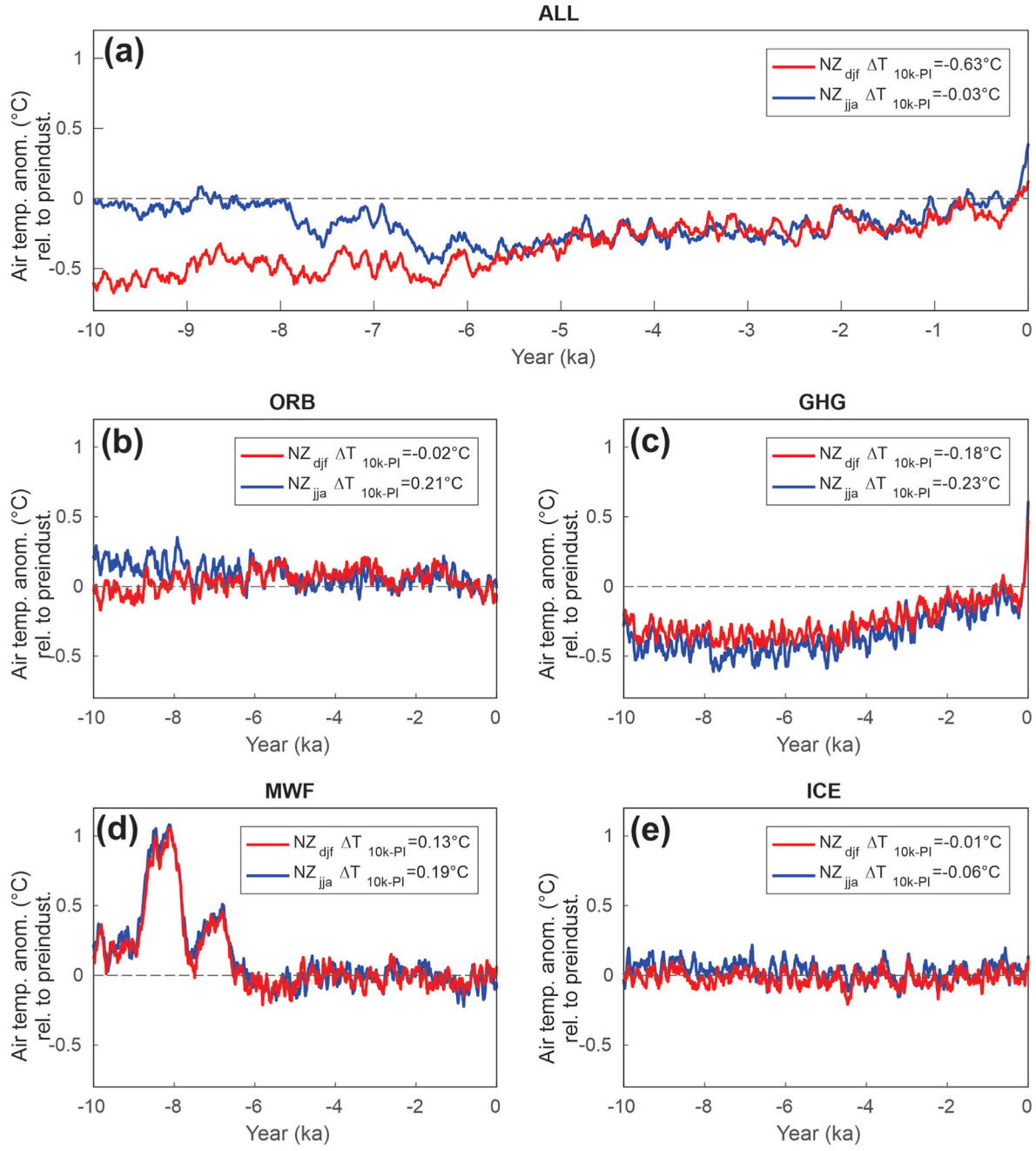

Fig. 7. Summer (DJF; red) and winter (JJA; blue) surface air temperature anomalies (relative to the 1820–1850 CE average) for South Island, New Zealand extracted from the TraCE-21k experiments conducted using the Community Climate System Model version 3 (CCSM3; He, 2011). Each plot corresponds to a different model integration: (a) 'ALL' includes all available forcings; (b–e) sensitivity runs driven by only orbital insolation (b; ORB), greenhouse gases (c; GHG), meltwater fluxes (d; MWF), and ice sheet geometry (e; ICE). (For interpretation of the references to colour in this figure legend, the reader is referred to the Web version of this article.)

experience a net rise of ~0.2 °C between 10 ka and the pre-industrial era (Fig. 7c). This change comprises a gradual cooling in the early Holocene imparted by a ~5 ppm decline in CO_2 between 11.5 and 7.4 ka, when temperatures are ~0.4 °C below pre-industrial levels. Between 7.5 ka and 0.5 ka, CO_2 increased by ~22 ppm, which causes New Zealand air temperatures in both seasons to increase by 0.3 °C during this interval (Fig. 7c). This greenhouse gas-induced warming pattern is also evident in the ALL-forcings simulation, which suggests that greenhouse gas forcing may have been an important driver of multi-millennial climate trends in New Zealand during the Holocene.

A prominent role for greenhouse gas forcing of regional temperatures in New Zealand during the Holocene is further supported by the agreement with the sign and temporal pattern of CCSM3 summer air temperature changes when compared to the composite mountain glacier moraine record (e.g. Fig. 6). A plateau of the coldest Holocene summer temperatures between 11 and 7 ka is consistent with glaciers generally being larger during this interval than at any time later in the interglacial. The onset of warming after 7 ka, driven by increasing greenhouse gases is also consistent with the near absence of mid-Holocene moraines in the Southern Alps. Furthermore, the greenhouse gas-driven temperature spike in the

20th century coincides with the interval during which 60% of the net Holocene decline of Dart Glacier occurs, with a similar retreat being observed elsewhere in the Southern Alps (Putnam et al., 2012; Purdie et al., 2014).

Fig. 7 shows that meltwater forcing in the TraCE-21k experiments has potential to impact air temperature in the New Zealand region, but only for the duration of meltwater discharge (Fig. 7d). Based on the prescription of meltwater to the TraCE-21k experiments, rapid and high amplitude millennial-scale warming events occur in the early Holocene in response to changing meltwater flux and/or location (He, 2011). These discrete events coincide with two meltwater pulse events prescribed in the vicinity of the Hudson Strait at 9–8 ka and 7.6–6.9 ka. The warming that New Zealand experienced at the same time as these meltwater pulses may reflect some of the physical mechanisms of the bipolar seesaw identified and described by Pedro et al. (2018).

In general, climate model studies have shown that freshwater applied to the Southern Ocean results in regional-to hemispheric-scale cooling (Weaver et al., 2003; Golledge et al., 2019). In the TraCE-21k experiments, Antarctic meltwater flux is held constant during the Holocene until 5 ka when it drops to zero. Removal of this freshwater flux at 5 ka may be seen in the MWF scenario as a slight rise in New Zealand air temperature, illustrating the potential impact that Antarctic meltwater can have on austral mid-latitude climate (Fig. 7). There is some evidence for discharge of Antarctic ice during the early Holocene (Small et al., 2019; Jones et al., 2021), which has the potential to contribute to the cool conditions inferred from the composite Southern Alps moraine record (Fig. 7). However, the total magnitude of ice sheet discharge during this time is unclear.

In summary, the early Holocene glacial maximum seen in moraine records of the Southern Alps, and elsewhere in the southern mid-latitudes, is consistent with the radiative forcing effects of weaker summer insolation intensity and reduced greenhouse gas concentrations in the TraCE-21k simulations. Our suggestion for the role of local insolation in driving regional temperature in New Zealand during the early Holocene contradicts other local moraine chronologies from the peak of the last glacial cycle, which find no relationship between glacier change and orbital forcing (e.g. Doughty et al., 2015; Strand et al., 2019). The influence of orbital forcing on regional temperatures may have been greater during the Holocene, relative to the glacial, due to the paucity of other competing climatic influences during the relatively stable interglacial. However, we stress that the absolute magnitude of temperature change imparted by insolation alone is fairly minor (e.g. Fig. 7), thus it is unlikely to be the sole cause of the net austral summertime warming and glacier retreat through the Holocene. At the very least, the GCM simulations do support the assertion that insolation forcing is a key contributor for the reduced seasonality previously interpreted from divergent climate-proxy reconstructions for the early Holocene (e.g. van den Bos et al., 2018).

While insolation may explain some of the seasonality differences seen in climate proxies, greater influence on regional temperature was likely imparted by the reduced atmospheric greenhouse gas concentrations of the early Holocene (Fig. 7). Net warming and glacier retreat through the interglacial is consistent with greenhouse gas forcing, which rose steadily after 7 ka, before accelerating in the 20th century. Therefore, while we agree in part with the suggestion of Reynhout et al. (2019) that local summer insolation may have paced austral climate during the Holocene, we suggest this influence may have been superseded by greenhouse gas forcing.

6. Conclusion

Using cosmogenic ^{10}Be surface exposure dating, we have extended the 100-year history of observational records at Dart Glacier, located in the Southern Alps of New Zealand, constraining the timing of moraine building events to 7.8 ± 0.3 ka and 321 ± 44 yr ago. Our findings are consistent with emerging evidence for an early Holocene glacial maximum in southern mid-latitudes and suggest the onset of regional-scale glacier retreat began around 7 ka, as indicated by a hiatus in the composite moraine record for the Southern Alps. Interpreting the regional composite of moraine chronologies using the framework of transient global climate model simulations, we identify key roles for local summer insolation and greenhouse gas forcing in dictating austral glacier and climate trends during the Holocene. In particular, we propose that greenhouse gas forcing, which is dominated by the radiative influence of carbon dioxide concentrations, may have played a larger role than presently accounted for, potentially driving long term warming and net glacier retreat since the mid-Holocene.

Credit author statement

Lisa Dowling: Conceptualization, Formal analysis, Investigation, Writing – original draft, Writing – review & editing, Visualization, Project administration, Shaun Eaves: Conceptualization, Formal analysis, Writing – original draft, Writing – review & editing, Visualization, Supervision, Funding acquisition, Project administration, Kevin Norton: Conceptualization, Writing – review & editing, Supervision, Funding acquisition, Project administration, Andrew Mackintosh: Conceptualization, Writing – review & editing, Funding acquisition, Brian Anderson: Conceptualization, Writing – review & editing, Funding acquisition, Alan Hidy: Investigation, Writing – review & editing, Andrew Lorrey: Conceptualization, Writing – review & editing, Funding acquisition, Lauren Vargo: Investigation, Writing – review & editing, Matt Ryan: Investigation, Writing – review & editing, Stephen Tims: Writing – review & editing, Funding acquisition.

Declaration of competing interest

The authors declare that they have no known competing financial interests or personal relationships that could have appeared to influence the work reported in this paper.

Acknowledgements

This study was supported by the National Geographic Society Waitt Foundation (W427-16) and the Royal Society of New Zealand Marsden Fund (fast-start contract VUW1605). L. Dowling acknowledges further support from the Victoria University of Wellington School of Geography Environment and Earth Sciences Master's Publication Scholarship and the Antarctic Research Centre's Endowed Development Fund. A. Lorrey was supported by the NIWA SSIF project “Climate Present and Past” contract CAOA2101. This work was performed in part under the auspices of the US Department of Energy by Lawrence Livermore National Laboratory, United States under Contract DE-AC52-07NA27344. This is LLNL-JRNL-815423.

Appendix A. Supplementary data

Supplementary data to this article can be found online at https://doi.org/10.1016/j.quascirev.2021.107068.

References

Bakke, J., Paasche, Ø., Schaefer, J.M., Timmermann, A., 2021. Long-term demise of sub-Antarctic glaciers modulated by the Southern Hemisphere Westerlies. Sci. Rep. 11 (1), 8361. https://doi.org/10.1038/s41598-021-87317-5.

Balco, G., 2006. Converting Al and Be isotope ratio measurements to nuclide concentrations in quartz. Retrieved from. http://hess.ess.washington.edu/math/docs/common/ams_data_reduction/.

Balco, G., 2017. The Online Exposure Age Calculator Formerly Known as the CRONUS-Earth Online Exposure Age Calculator. Retrieved from. https://hess.ess.washington.edu/math/v3/v3_age_in.html.

Balco, G., 2020. glacier change and paleoclimate applications of cosmogenic-nuclide exposure dating. Annu. Rev. Earth Planet Sci. 48 (1), 21–48. https://doi.org/10.1146/annurev-earth-081619-052609.

Balco, G., Stone, J.O., Lifton, N.A., Dunai, T.J., 2008. A complete and easily accessible means of calculating surface exposure ages or erosion rates from 10Be and 26Al measurements. Quat. Geochronol. 3 (3), 174–195. https://doi.org/10.1016/j.quageo.2007.12.001.

Barrell, D., Andersen, B., Denton, G., 2011. Glacial geomorphology of the central South Island, New Zealand. GNS Sci. Monogr. 27 (81).

Barrell, D.J.A., 2011. Quaternary glaciers of New Zealand. Dev. Quat. Sci. 15, 1047–1064. https://doi.org/10.1016/B978-0-444-53447-7.00075-1.

Baumann, S., Anderson, B., Chinn, T., Mackintosh, A., Collier, C., Lorrey, A.M., Rack, W., Purdie, H., Eaves, S., 2020. Updated inventory of glacier ice in New Zealand based on 2016 satellite imagery. J. Glaciol. 1–14. https://doi.org/10.1017/jog.2020.78.

Bishop, G., Forsyth, J., 1988. Vanishing ice: an introduction to glaciers based on a study of the Dart Glacier. John McIndoe and New Zealand Geological Survey, DSIR, Dunedin, New Zealand.

Borchers, B., Marrero, S., Balco, G., Caffee, M., Goehring, B., Lifton, N., Nishiizumi, K., Phillips, F., Schaefer, J., Stone, J., 2016. Geological calibration of spallation production rates in the CRONUS-Earth project. Quat. Geochronol. 31, 188–198. https://doi.org/10.1016/j.quageo.2015.01.009.

Burrows, C., Maunder, B., 1975. The recent moraines of the Lyell and Ramsay glaciers Rakaia valley, Canterbury. J. Roy. Soc. N. Z. 5 (4), 479–491. https://doi.org/10.1080/03036758.1975.10419364.

Doughty, A.M., Schaefer, J.M., Putnam, A.E., Denton, G.H., Kaplan, M.R., Barrell, D.J.A., Andersen, B.G., Kelley, S.E., Finkel, R.C., Schwartz, R., 2015. Mismatch of glacier extent and summer insolation in Southern Hemisphere mid-latitudes. Geology 43 (5), 407–410. https://doi.org/10.1130/G36477.1.

Douglass, D.C., Singer, B.S., Kaplan, M.R., Ackert, R.P., Mickelson, D.M., Caffee, M.W., 2005. Evidence of early Holocene glacial advances in southern South America from cosmogenic surface-exposure dating. Geology 33 (3), 237–240. https://doi.org/10.1130/G21144.1.

Eaves, S.R., Winckler, G., Mackintosh, A.N., Schaefer, J.M., Townsend, D.B., Doughty, A.M., Jones, R.S., Leonard, G.S., 2019. Late-glacial and Holocene glacier fluctuations in North Island, New Zealand. Quat. Sci. Rev. 223, 105914 https://doi.org/10.1016/j.quascirev.2019.105914.

Golledge, N.R., Keller, E.D., Gomez, N., Naughten, K.A., Bernales, J., Trusel, L.D., Edwards, T.L., 2019. Global environmental consequences of twenty-first-century ice-sheet melt. Nature 566 (7742), 65–72. https://doi.org/10.1038/s41586-019-0889-9.

Hall, B.L., Lowell, T.V., Bromley, G.R.M., Denton, G.H., Putnam, A.E., 2019. Holocene glacier fluctuations on the northern flank of Cordillera Darwin, southernmost South America. Quat. Sci. Rev. 222, 105904 https://doi.org/10.1016/j.quascirev.2019.105904.

Harrison, S., Glasser, N.F., Duller, G.A.T., Jansson, K.N., 2012. Early and mid-Holocene age for the tempanos moraines, Laguna san rafael, patagonian Chile. Quat. Sci. Rev. 31, 82–92. https://doi.org/10.1016/j.quascirev.2011.10.015.

He, F., 2011. *Simulating Transient Climate Evolution of the Last Deglaciation with CCSM3.* (PhD). University of Wisconsin-Madison, Madison, WI, United States.

Jones, J.M., Gille, S.T., Goosse, H., Abram, N.J., Canziani, P.O., Charman, D.J., Clem, K.R., Crosta, X., de Lavergne, C., Eisenman, I., England, M.H., Fogt, R.L., Frankcombe, L.M., Marshall, G.J., Masson-Delmotte, V., Morrison, A.K., Orsi, A.J., Raphael, M.N., Renwick, J.A., Schneider, D.P., Simpkins, G.R., Steig, E.J., Stenni, B., Swingedouw, D., Vance, T.R., 2016. Assessing recent trends in high-latitude Southern Hemisphere surface climate. Nat. Clim. Change 6 (10), 917–926. https://doi.org/10.1038/nclimate3103.

Jones, R.S., Mackintosh, A.N., Norton, K.P., Golledge, N.R., Fogwill, C.J., Kubik, P.W., Christl, M., Greenwood, S.L., 2015. Rapid Holocene thinning of an East Antarctic outlet glacier driven by marine ice sheet instability. Nat. Commun. 6 (1), 8910. https://doi.org/10.1038/ncomms9910.

Jones, R.S., Whitmore, R.J., Mackintosh, A.N., Norton, K.P., Eaves, S.R., Stutz, J., Christl, M., 2021. Regional-scale abrupt Mid-Holocene ice sheet thinning in the western Ross Sea, Antarctica. Geology 49 (3), 278–282. https://doi.org/10.1130/G48347.1.

Joos, F., Spahni, R., 2008. Rates of change in natural and anthropogenic radiative forcing over the past 20,000 years. Proc. Natl. Acad. Sci. Unit. States Am. 105 (5), 1425–1430. https://doi.org/10.1073/pnas.0707386105.

Kaplan, M.R., Schaefer, J.M., Denton, G.H., Doughty, A.M., Barrell, D.J.A., Chinn, T.J.H., Putnam, A.E., Andersen, B.G., Mackintosh, A., Finkel, R.C., Schwartz, R., Anderson, B., 2013. The anatomy of long-term warming since 15 ka in New Zealand based on net glacier snowline rise. Geology 41 (8), 887–890. https://doi.org/10.1130/g34288.1.

Kaplan, M.R., Schaefer, J.M., Strelin, J.A., Denton, G.H., Anderson, R.F., Vandergoes, M.J., Finkel, R.C., Schwartz, R., Travis, S.G., Garcia, J.L., Martini, M.A., Nielsen, S.H.H., 2016. Patagonian and southern South Atlantic view of Holocene climate. Quat. Sci. Rev. 141, 112–125. https://doi.org/10.1016/j.quascirev.2016.03.014.

Lifton, N., Sato, T., Dunai, T.J., 2014. Scaling in situ cosmogenic nuclide production rates using analytical approximations to atmospheric cosmic-ray fluxes. Earth Planet Sci. Lett. 386, 149–160. https://doi.org/10.1016/j.epsl.2013.10.052.

Lorrey, A., Bostock, H., 2017. The Quaternary climate of New Zealand. In: Shulmeister, J. (Ed.), Landscape and Quaternary Environmental Change in New Zealand. Atlantic Press, Paris, pp. 67–139.

Lorrey, A., Fauchereau, N., Stanton, C., Chappell, P., Phipps, S., Mackintosh, A., Renwick, J., Goodwin, I., Fowler, A., 2014. The Little Ice Age climate of New Zealand reconstructed from Southern Alps cirque glaciers: a synoptic type approach. Clim. Dynam. 42 (11), 3039–3060. https://doi.org/10.1007/s00382-013-1876-8.

Lorrey, A.M., Williams, P.W., Woolley, J.-M., Fauchereau, N.C., Hartland, A., Bostock, H., Eaves, S., Lachniet, M.S., Renwick, J.A., Varma, V., 2020. Late quaternary climate variability and change from Aotearoa New Zealand speleothems: progress in age modelling, oxygen isotope master record construction and proxy-model comparisons. Quaternary 3 (3), 24. https://doi.org/10.3390/quat3030024.

Mackintosh, A.N., Anderson, B.M., Lorrey, A.M., Renwick, J.A., Frei, P., Dean, S.M., 2017a. Regional cooling caused recent New Zealand glacier advances in a period of global warming. Nat. Commun. 8, 14202 https://doi.org/10.1038/ncomms14202.

Mackintosh, A.N., Anderson, B.M., Pierrehumbert, R.T., 2017b. Reconstructing climate from glaciers. Annu. Rev. Earth Planet Sci. 45 (1), 649–680. https://doi.org/10.1146/annurev-earth-063016-020643.

Marcott, S.A., Shakun, J.D., Clark, P.U., Mix, A.C., 2013. A reconstruction of regional and global temperature for the past 11,300 years. Science 339 (6124), 1198. https://doi.org/10.1126/science.1228026.

Masson, V., Vimeux, F., Jouzel, J., Morgan, V., Delmotte, M., Ciais, P., Hammer, C., Johnsen, S., Lipenkov, V.Y., Mosley-Thompson, E., Petit, J.-R., Steig, E.J., Stievenard, M., Vaikmae, R., 2000. Holocene climate variability in Antarctica based on 11 ice-core isotopic records. Quat. Res. 54 (3), 348–358. https://doi.org/10.1006/qres.2000.2172.

McColl, S.T., Cook, S.J., Stahl, T., Davies, T.R.H., 2019. Origin and age of the Hillocks and implications for post-glacial landscape development in the upper Lake Wakatipu catchment, New Zealand. J. Quat. Sci. 34 (8), 685–696. https://doi.org/10.1002/jqs.3168.

McGlone, M.S., Hall, G.M.J., Wilmshurst, J.M., 2010a. Seasonality in the early Holocene: extending fossil-based estimates with a forest ecosystem process model. Holocene 21 (4), 517–526. https://doi.org/10.1177/0959683610385717.

McGlone, M.S., Turney, C.S., Wilmshurst, J.M., Renwick, J., Pahnke, K., 2010b. Divergent trends in land and ocean temperature in the Southern Ocean over the past 18,000 years. Nat. Geosci. 3 (9), 622. https://doi.org/10.1038/ngeo931.

Menounos, B., Clague, J.J., Osborn, G., Davis, P.T., Ponce, F., Goehring, B., Maurer, M., Rabassa, J., Coronato, A., Marr, R., 2013. Latest Pleistocene and Holocene glacier fluctuations in southernmost Tierra del Fuego, Argentina. Quat. Sci. Rev. 77, 70–79. https://doi.org/10.1016/j.quascirev.2013.07.008.

Nishiizumi, K., Imamura, M., Caffee, M.W., Southon, J.R., Finkel, R.C., McAninch, J., 2007. Absolute calibration of 10Be AMS standards. Nucl. Instrum. Methods Phys. Res. Sect. B Beam Interact. Mater. Atoms 258 (2), 403–413. https://doi.org/10.1016/j.nimb.2007.01.297.

Oerlemans, J., 2001. Glaciers and Climate Change. A.A. Balkema, Lisse.

Oerlemans, J., Fortuin, J.P.F., 1992. Sensitivity of glaciers and small ice caps to greenhouse warming. Science 258 (5079), 115–117.

Oerlemans, J., Reichert, B.K., 2000. Relating glacier mass balance to meteorological data by using a seasonal sensitivity characteristic. J. Glaciol. 46 (152), 1–6. https://doi.org/10.3189/172756500781833269.

Pedro, J.B., Jochum, M., Buizert, C., He, F., Barker, S., Rasmussen, S.O., 2018. Beyond the bipolar seesaw: toward a process understanding of interhemispheric coupling. Quat. Sci. Rev. 192, 27–46. https://doi.org/10.1016/j.quascirev.2018.05.005.

Prebble, J.G., Bostock, H.C., Cortese, G., Lorrey, A.M., Hayward, B.W., Calvo, E., Northcote, L.C., Scott, G.H., Neil, H.L., 2017. Evidence for a Holocene climatic optimum in the southwest pacific: a multiproxy study. Paleoceanography 32 (8), 763–779. https://doi.org/10.1002/2016PA003065.

Purdie, H., Anderson, B., Chinn, T., Owens, I., Mackintosh, A., Lawson, W., 2014. Franz Josef and Fox glaciers, New Zealand: historic length records. Global Planet. Change 121, 41–52. https://doi.org/10.1016/j.gloplacha.2014.06.008.

Putnam, A.E., Schaefer, J.M., Barrell, D.J.A., Vandergoes, M., Denton, G.H., Kaplan, M.R., Finkel, R.C., Schwartz, R., Goehring, B.M., Kelley, S.E., 2010. In situ cosmogenic 10Be production-rate calibration from the Southern Alps, New Zealand. Quat. Geochronol. 5 (4), 392–409. https://doi.org/10.1016/j.quageo.2009.12.001.

Putnam, A.E., Schaefer, J.M., Denton, G.H., Barrell, D.J.A., Finkel, R.C., Andersen, B.G., Schwartz, R., Chinn, T.J.H., Doughty, A.M., 2012. Regional climate control of glaciers in New Zealand and Europe during the pre-industrial Holocene. Nat. Geosci. 5 (9), 627–630. https://doi.org/10.1038/ngeo1548.

Reynhout, S.A., Sagredo, E.A., Kaplan, M.R., Aravena, J.C., Martini, M.A., Moreno, P.I., Rojas, M., Schwartz, R., Schaefer, J.M., 2019. Holocene glacier fluctuations in Patagonia are modulated by summer insolation intensity and paced by Southern Annular Mode-like variability. Quat. Sci. Rev. 220, 178–187. https://

doi.org/10.1016/j.quascirev.2019.05.029.
Ruddell, A.R., 1995. Recent Glacier and Climate Change in the New Zealand Alps. (PhD). Retrieved from. University of Melbourne, Australia. http://hdl.handle.net/11343/39107.
Schaefer, J.M., Denton, G.H., Kaplan, M., Putnam, A., Finkel, R.C., Barrell, D.J.A., Andersen, B.G., Schwartz, R., Mackintosh, A., Chinn, T., Schlüchter, C., 2009. High-frequency Holocene glacier fluctuations in New Zealand differ from the northern signature. Science 324 (5927), 622–625. https://doi.org/10.1126/science.1169312.
Schimmelpfennig, I., Schaefer, J.M., Akçar, N., Koffman, T., Ivy-Ochs, S., Schwartz, R., Finkel, R.C., Zimmerman, S., Schlüchter, C., 2014. A chronology of Holocene and Little Ice Age glacier culminations of the Steingletscher, Central Alps, Switzerland, based on high-sensitivity beryllium-10 moraine dating. Earth Planet Sci. Lett. 393, 220–230. https://doi.org/10.1016/j.epsl.2014.02.046.
Small, D., Bentley, M.J., Jones, R.S., Pittard, M.L., Whitehouse, P.L., 2019. Antarctic ice sheet palaeo-thinning rates from vertical transects of cosmogenic exposure ages. Quat. Sci. Rev. 206, 65–80. https://doi.org/10.1016/j.quascirev.2018.12.024.
Sommerville, P., Mark, A.F., Wilson, J.B., 1982. Plant succession on moraines of the upper Dart valley, southern South Island, New Zealand. N. Z. J. Bot. 20 (3), 227–244. https://doi.org/10.1080/0028825X.1982.10428492.
Stone, J., 2000. Air pressure and cosmogenic isotope production. J. Geophys. Res.: Solid Earth 105 (B10), 23753–23759. https://doi.org/10.1029/2000JB900181.
Strand, P.D., Schaefer, J.M., Putnam, A.E., Denton, G.H., Barrell, D.J.A., Koffman, T.N.B., Schwartz, R., 2019. Millennial-scale pulsebeat of glaciation in the southern Alps of New Zealand. Quat. Sci. Rev. 220, 165–177. https://doi.org/10.1016/j.quascirev.2019.07.022.
Strelin, J.A., Kaplan, M.R., Vandergoes, M.J., Denton, G.H., Schaefer, J.M., 2014. Holocene glacier history of the Lago Argentino basin, southern patagonian icefield. Quat. Sci. Rev. 101, 124–145. https://doi.org/10.1016/j.quascirev.2014.06.026.
Tait, A., Henderson, R., Turner, R., Zheng, X., 2006. Thin plate smoothing spline interpolation of daily rainfall for New Zealand using a climatological rainfall surface. Int. J. Climatol. 26 (14), 2097–2115. https://doi.org/10.1002/joc.1350.
Turnbull, I.M., 2000. Geology of the Wakatipu Area: Scale 1:250,000. Lower Hutt: Institute of Geological & Nuclear Sciences.
van den Bos, V., Rees, A., Newnham, R., Vandergoes, M., Wilmshurst, J., Augustinus, P., 2018. Holocene temperature, humidity and seasonality in northern New Zealand linked to Southern Hemisphere summer insolation. Quat. Sci. Rev. 201, 77–88. https://doi.org/10.1016/j.quascirev.2018.10.008.
Weaver, A.J., Saenko, O.A., Clark, P.U., Mitrovica, J.X., 2003. Meltwater pulse 1A from Antarctica as a trigger of the Bølling-Allerød Warm interval. Science 299 (5613), 1709–1713. https://doi.org/10.1126/science.1081002.
Wenzens, G., 1999. Fluctuations of outlet and valley glaciers in the southern Andes (Argentina) during the past 13,000 years. Quat. Res. 51 (3), 238–247. https://doi.org/10.1006/qres.1999.2043.
Wilmshurst, J.M., McGlone, M.S., Leathwick, J.R., Newnham, R.M., 2007. A pre-deforestation pollen-climate calibration model for New Zealand and quantitative temperature reconstructions for the past 18 000 years BP. J. Quat. Sci. 22 (5), 535–547. https://doi.org/10.1002/jqs.1135.
Winkler, S., 2014. Investigation of late-Holocene moraines in the western Southern Alps, New Zealand, applying Schmidt-hammer exposure-age dating. Holocene 24 (1), 48–66. https://doi.org/10.1177/0959683613512169.
Wright, H.F., 1921. The late major Bernard head's last Dart expedition. N. Z. Alpine J. 3 (11), 86–89.